Upper tropospheric temperature measurements with the use of a Raman lidar

Keith D. Evans, S. Harvey Melfi, Richard A. Ferrare, and David N. Whiteman

Upper tropospheric temperature profiles were measured with the NASA Goddard Space Flight Center scanning Raman lidar five months after the eruption of Mt. Pinatubo. To derive temperatures in regions of high aerosol content, the aerosol transmission is calculated for the Raman N_2 return signals under cloud-free conditions. The lidar-derived aerosol backscattering ratio and an estimate of the aerosol extinction-to-backscatter ratio were used to compute the aerosol transmission. With a model reference temperature at 25 km, temperature profiles with a root-mean-square difference between the lidar and radiosonde temperatures of <2 K were obtained over an altitude range of 5–10 km for a 10-min integrated measurement with 300-m resolution.

Key words: Temperature profile, Raman lidar, aerosol transmission.

1. Introduction

The Goddard Space Flight Center (GSFC) scanning Raman lidar (SRL) was completed in October 1991. This system was designed for and has made measurements of the tropospheric water vapor mixing ratio and the corresponding aerosol backscattering ratio.[1] The Mt. Pinatubo aerosol layer has also been measured.[2] Atmospheric temperature profile measurements are presented here.

Previously, most lidar atmospheric temperature profile measurements[3–19] have been made in the stratosphere and mesosphere, above approximately 30 km, with Rayleigh backscattering in a region where the aerosol content of the atmosphere is negligible. A number density profile is determined from the Rayleigh backscattered signal and then used to calculate a temperature profile. This method assumes that, above 30 km, the molecular extinction versus altitude is constant. Below 30 km, the molecular extinction cannot be assumed constant. Here the variation of molecular transmission with altitude cannot be neglected. Temperature measurements have been made through the lower stratosphere and into the troposphere with Raman rotational[20,21] scattering, which is unaffected by aerosols, and with Raman vibrational[22–24] scattering when aerosol attenuation could be neglected. These methods had temperature errors of ≤ 1 K.

Major volcanic eruptions inject aerosols into the lower stratosphere. After such eruptions, and in the following months, aerosol attenuation, as molecular attenuation, cannot be neglected. Several methods to correct for attenuation by aerosols have been used to obtain a temperature profile. One method separates the Mie scattering contribution by the use of an atomic blocking filter to derive temperatures within 10 °K of radiosonde temperatures.[25] Another method[26] uses the Bernoulli solution to the lidar equation[27] to determine the aerosol extinction to derive temperatures with 5 K random error but only in the lower troposphere. A third method uses the Raman scattering from nitrogen molecules corrected for Mie and Rayleigh scattering with a statistical database of lidar measurements of the post-Mt. St. Helen's stratospheric aerosols to calculate the aerosol attenuation when the attenuation was $<10\%$.[28]

The key to obtaining temperature profiles is to obtain a number density profile that is proportional to the atmospheric number density. In this paper we demonstrate a method for calculating number densities in the lower stratosphere after the eruption of a

When this research was undertaken K. D. Evans and R. A. Ferrare were at Hughes STX Corporation, Lanham, Maryland, under contract at NASA Goddard Space Flight Center, Code 912, Greenbelt, Maryland 20771. S. H. Melfi and D. N. Whiteman were in Codes 917 and 924, respectively, at NASA Goddard Space Flight Center, Greenbelt, Maryland 20771. Currently, K. D. Evans is at the Joint Center for Earth Systems Technology and S. H. Melfi is with the Department of Physics, both at the University of Maryland Baltimore County, 5401 Wilkins Avenue, Baltimore, Maryland 21228.

Received 2 January 1996; revised manuscript received 24 September 1996.

0003-6935/97/122594-09$10.00/0

major volcano, such as Mt. Pinatubo. We utilized the lidar-derived aerosol backscattering ratio, which is defined as the ratio of total (aerosol and molecular) backscatter to molecular backscatter, in calculating the aerosol transmission of the lidar signals so as to obtain a more accurate number density through the lower stratosphere. Thereafter, the temperature profile can be determined.

The Raman lidar system is described in Section 2, followed by a discussion of the data used to demonstrate this method. We present a synopsis of the method used for deriving temperatures above 30 km, where molecular attenuation can be approximated as a constant, followed by a detailed discussion of the molecular and aerosol attenuation transmissions applied below 30 km and how this algorithm is adapted for our system. The resulting temperature and density profiles are presented with a discussion of the errors and a sensitivity analysis of this method. Conclusions are presented in Section 7.

2. System Description

The SRL is a trailer-based system[2] that uses a XeF excimer laser to transmit light at 351 nm. The system operates at 400 Hz with 30 mJ per pulse for an average output of 12 W in the far field. A 0.76-m Dall–Kirkham telescope gathers the laser return and the vibrational Raman-shifted returns from O_2 (372 nm), N_2 (383 nm), and H_2O (403 nm) gas molecules. Beam splitters separate the return beam into low- and high-sensitivity channels for each wavelength so as to extend the measurement range of the lidar system. The collected light is then photon counted with 100-MHz bandwidth electronics. The data are saved in the form of 1-min contiguous profiles that possess an altitude resolution of 75 m.

We focus this analysis on the high-sensitivity data only because the high-sensitivity data have a higher signal-to-noise (S/N) ratio than the low-sensitivity data. The high-sensitivity channel is count saturated in the lowest few kilometers. Therefore, the temperature profile minimum altitude will vary from 4 to 5 km depending on the altitude when the count saturation of the photomultiplier tubes can be corrected accurately to the true counts.[29]

3. Data

The SRL was first deployed at the Coffeyville, Kansas, airport (37.10 °N, 95.57 °W) as part of the FIRE-II [First ISCCP (International Satellite Cloud Climatology Project) Regional Experiment-II] and SPECTRE (Spectral Radiance Experiment) campaigns, which occurred simultaneously from 13 November to 7 December 1991. Although 14 nights of data were collected, only 10 were used here because the presence of significant clouds limited the maximum altitude of the laser return signals.

The 1-min data have been summed for 10 min and smoothed to a 300-m altitude resolution. A total of 53 10-min profiles over 10 nights were used for gathering statistics. Although the SRL has the capability of collecting daytime data,[30] only nighttime data are presented here because the daytime data are limited to the lower troposphere. No scanning data are used for our research in this paper.

Radiosondes were launched from two sites. One was at the Coffeyville airport approximately 100 m from the SRL site. The other launch site was approximately 0.5 km northwest of the lidar site. The radiosondes were launched every 2–4 h during the FIRE-II and SPECTRE operations. Sixty-six radiosondes were launched specifically for the experiment and were not part of the standard 12-h radiosonde network. Radiosonde temperature data are used for comparison with the lidar-derived temperatures.

4. Temperature Algorithm

A. Theory

The equations for number density and temperature were derived previously,[3,6] and a synopsis follows. The atmospheric number density profile $n(z)$ is obtained as follows:

$$n(z) = n(z_h)\frac{P(z)}{P(z_h)}\, q_R(\lambda_0, z, z_h) q_R(\lambda_N, z, z_h) \times q_A(\lambda_0, z, z_h) q_A(\lambda_N, z, z_h), \quad (1)$$

where z is the altitude, z_h is the altitude of the reference number density, $P(z)$ is the range-squared signal counts, λ_0 is the laser wavelength, λ_N is the return wavelength, $q_R(\lambda, z, z_h)$ is the one-way molecular transmission, and $q_A(\lambda, z, z_h)$ is the one-way aerosol transmission. For completeness, aerosol transmission is included in these equations and are explained in Subsection 4.B. The last two terms in Eq. (1) are given by

$$q_R(\lambda, z, z_h) = \exp\left[-\sigma_R(\lambda)\int_z^{z_h} n(x)\mathrm{d}x\right], \quad (2)$$

$$q_A(\lambda, z, z_h) = \exp\left[-\int_z^{z_h} \alpha_A(\lambda, x)\mathrm{d}x\right], \quad (3)$$

where x is the variable of integration (altitude, in this case), $\sigma_R(\lambda)$ is the Rayleigh attenuation cross section as a function of wavelength, $n(x)$ is the molecular number density, and $\alpha_A(\lambda, x)$ is the aerosol extinction coefficient. We obtained a first guess for the number density using the hypsometric equation and the reference (at the isopycnic level, see below) or a previously calculated number density. This first guess is used to calculate the molecular and aerosol transmissions. Then a new number density is obtained with Eq. (1). This process is iterated until the change between the input and the calculated number densities is less than 1%. Normalizing the number density to a reference number density allows us to determine an absolute number density.

Assuming hydrostatic equilibrium and using the ideal gas law, we can calculate a temperature profile that corresponds to the number density profile. The number density profile is normalized to a reference

temperature at the top of the density profile. The temperature profile $T(z)$ is computed with

$$T(z) = \frac{n(z_r)}{n(z)}\,T(z_r) + \frac{m}{k}\int_z^{z_r} \frac{n(x)}{n(z)}\,g(x)\mathrm{d}x, \qquad (4)$$

where $n(z)$ is the number density, z_r is the altitude of the reference temperature, $T(z_r)$ is the reference temperature, m is the average mass of an air molecule, k is Boltzmann's constant, and $g(x)$ is the acceleration due to gravity. As the calculation proceeds downward with respect to altitude, the first term on the right-hand side of Eq. (4) becomes small and the second term dominates. The calculated temperature has <1% error that is due to the reference temperature after approximately 10–15 km (Ref. 3). This is not true if the calculation proceeds upward in altitude. Thus it is desirable to have a reference temperature at the highest possible altitude.

B. Lidar Methods

For temperatures at altitudes above 30 km, where the stratospheric aerosol layer is normally negligible, $q_A(\lambda, z, z_h) = 1$, and the molecular transmission $q_R(\lambda, z, z_h)$ can be assumed to be constant to within 0.4% (Ref. 3) accuracy. In the above algorithm, if $\lambda_0 = \lambda_N$, where λ_0 is the laser wavelength, then this becomes the Rayleigh lidar method.

To obtain temperatures below 30 km, the Rayleigh method must be modified. At altitudes below 30 km, the molecular scattering increases rapidly, and molecular transmission cannot be assumed constant. The molecular transmission is given by

$$q_R{}^2(\lambda_0, z, z_h) = \exp\left[-2\sigma_R(\lambda_0)\int_z^{z_h} n(x)\mathrm{d}x\right]. \qquad (5)$$

The number density is integrated from the altitude of calculation z to the reference number density altitude z_h and multiplied by the Rayleigh scattering cross section. This method can be used when there are little or no aerosols in the atmosphere.

A Raman lidar uses the nitrogen signal in the determination of the number density, so that the laser and return wavelengths are different and both must be accounted for in the molecular transmission term. The molecular transmission is now given by

$$q_R(\lambda_0, z, z_h)q_R(\lambda_N, z, z_h) = \exp\left\{-[\sigma_R(\lambda_0) + \sigma_R(\lambda_N)]\int_z^{z_h} n(x)\mathrm{d}x\right\}. \qquad (6)$$

Here λ_N is the nitrogen wavelength.

After major volcanic eruptions, such as the Mt. Pinatubo eruption in June 1991, there can be a large aerosol content in the lower stratosphere. At these times, the aerosol transmission cannot be assumed to be 1 and must be calculated. This calculation is the essence of our research in this paper.

With a Raman lidar, both the output and the return wavelengths are different, and therefore the aerosol transmission is given by

$$q_A(\lambda_0, z, z_h)q_A(\lambda_N, z, z_h) = \exp\left\{-\int_z^{z_h}[\alpha_A(\lambda_0, x) + \alpha_A(\lambda_N, x)]\mathrm{d}x\right\}, \qquad (7)$$

$$\alpha_A(\lambda_0, x) = \frac{3}{8\pi}\,S_A(x)\sigma_R(\lambda_0) \times [R(\lambda_0, x) - 1]n(x), \qquad (8)$$

$$\alpha_A(\lambda_N, x) = \left(\frac{\lambda_0}{\lambda_N}\right)^{\gamma}\alpha_A(\lambda_0, x), \qquad (9)$$

where $\alpha_A(\lambda_0, x)$ is the aerosol extinction coefficient at the laser wavelength, $S_A(x)$ is the aerosol extinction-to-backscatter ratio (also known as and hereafter referred to as the lidar ratio), $R(\lambda_0, x)$ is the aerosol backscattering ratio [(molecular + aerosol scattering)/molecular scattering], $\alpha_A(\lambda_N, x)$ is the aerosol extinction coefficient at the nitrogen wavelength, and γ is the wavelength dependence of aerosol backscattering. The SRL measures the aerosol backscattering at the laser wavelength λ_0, but to obtain the aerosol backscattering at the nitrogen wavelength λ_N, a wavelength correction is applied to the aerosol backscattering at the laser wavelength. A value of $\gamma = 1$ is used to relate the aerosol extinction between the two wavelengths for small aerosol particles approximately the size of the laser wavelength.[31]

The aerosol backscattering ratio is derived with the ratio of the laser return signal counts divided by the nitrogen signal counts. This ratio is a measure of the Rayleigh plus Mie scattering to the Rayleigh scattering, such that, ratio values of 1 mean that there is no Mie scattering, and higher values signify the amount of Mie scattering. A minimum ratio value is determined in an altitude region of 6–10 km of cloud-free data, and the ratio profile is normalized to this minimum value. The data show a nearly constant aerosol backscattering ratio in this altitude range which implies that the aerosol backscattering at 351 nm is negligible.[2] Figure 1 shows the aerosol backscattering ratio profile for 19 November 1991, 0301–0310 UT; note the high scattering ratios around 20–22 km. The aerosol backscattering ratio needs to be determined first before this temperature algorithm is applied.

The only unknown remaining in Eqs. (7–9) is the aerosol extinction-to-backscatter ratio $S_A(x)$, which we call the lidar ratio. The extinction and backscatter components of the lidar ratio $S_A(x)$ were estimated separately and then divided to obtain an estimate of the average lidar ratio through the lower stratospheric aerosol layer. The lidar ratio has to be determined before the number density can be iterated, and, therefore, a model number density is used

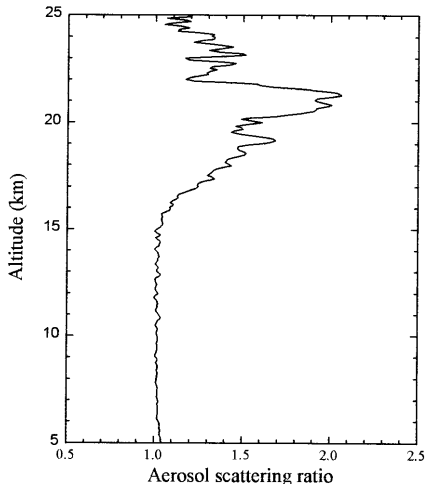

Fig. 1. Lidar-derived aerosol backscattering ratio for 19 November 1991, 0301–0310 UT. Note the large scattering ratio between 20–22 km caused by the Mt. Pinatubo eruption.

for the lidar ratio calculation. Solving Eq. (1) for the aerosol transmission and assuming

$$q_A(\lambda_0, z_1, z_2) q_A(\lambda_N, z_1, z_2) = \exp[-2\tau_A(z_1, z_2)], \quad (10)$$

where z_1 and z_2 have been substituted for z and z_h, and using a model number density $n_m(z)$, we estimated the one-way aerosol optical depth through the lower stratosphere $\tau_A(z_1, z_2)$ as

$$\tau_A(z_1, z_2) = -\frac{1}{2} \ln\left\{\left[\frac{P(z_2)}{P(z_1)} \frac{n_m(z_1)}{n_m(z_2)}\right] \times q_R(\lambda_0, z_2, z_1) q_R(\lambda_N, z_2, z_1)\right\}. \quad (11)$$

Equation (11) cannot be used directly to compensate for aerosol transmission because the number density is required for this equation, and we have not yet derived the number density. Therefore we use a model number density for this equation. Gaseous absorption at the Raman nitrogen wavelength is assumed to be negligible.

The backscatter component of the lidar ratio is the integrated aerosol backscattering ratio through the stratospheric aerosol layer observed by the Raman lidar. The aerosol-integrated backscatter coefficient $\beta(z_1, z_2)$ is given by

$$\beta(z_1, z_2) = \left[1 + \left(\frac{\lambda_0}{\lambda_N}\right)^{\gamma}\right] \frac{3}{8\pi} \sigma_R(\lambda_0) \times \int_{z_1}^{z_2} [R(\lambda_0, x) - 1] n_m(x) \mathrm{d}x. \quad (12)$$

The number densities used in Eqs. (11) and (12) are model number densities that came from the U.S. Standard Atmosphere 1976[32] (USSA76) model number density.

We obtained an estimate for the lidar ratio $[S_A(x) = \tau_A(z_1, z_2)/\beta(z_1, z_2)]$ by dividing Eq. (11) by Eq. (12). Although the lidar ratio is altitude dependent, for our research in this paper it was assumed to be constant for all altitudes. This will not affect the number densities derived at altitudes where there are no aerosols, but may effect the number density calculations at altitudes where there are aerosols or clouds. Tropospheric aerosols typically have a different lidar ratio than stratospheric aerosols.[31] Therefore lidar data with upper tropospheric aerosols and/or clouds were not used here. The value of the lidar ratio may be different for different seasons.

Temperatures were calculated in 75-m bins, which were then smoothed to a 300-m resolution with a nearly equal ripple filter[33] to reduce the random error. Measurement errors at each altitude were derived with Poisson statistics where the standard deviation equals the square root of the signal counts. These errors were then propagated through the equations[34] to obtain temperature errors in degrees.

There are alternative methods to account for aerosol transmission, but the particular method presented here gave the smallest rms differences. Instead of the aerosol backscattering ratio, the aerosol extinction profile could be calculated and used for the aerosol transmission term [see Eqs. (3) and (8)]. Temperatures derived with the aerosol extinction profile looked as if the aerosol backscattering was not applied in the aerosol transmission. Another method that could be used is to derive the aerosol extinction profile, estimate the aerosol backscattering profile with the lidar ratio, and then use the laser elastic returns for computation of the number density profile. Because the aerosol extinction-to-backscatter ratio is dependent on altitude, different extinction-to-backscatter ratios would have to be used for different altitudes. We believe that this method would lead to larger rms differences than the method chosen, therefore this third alternative method was not used.

The next section discusses the reference data used for the calculations and the results of this method to calculate temperatures.

5. Results

A. Reference Data

For independent temperature profiles, we desire a reference number density that is independent of radiosonde measurements. To determine such a reference, density data from the 66 radiosonde launches are plotted in Fig. 2. All the radiosonde number density data were interpolated to the same altitudes and weighted by the number of balloons that had data at each altitude, because the radiosondes had different maximum altitudes. The standard deviation was a minimum over an altitude range of 7.30–7.95 km mean sea level. The isopycnic level (altitude of minimum latitudinal and seasonal molecular density variability) from the USSA76 number densities is approximately 7.95 km.[32] Therefore the number densities were normalized with the USSA76 number density at 7.95 km to obtain a measure of the real atmospheric number densities.

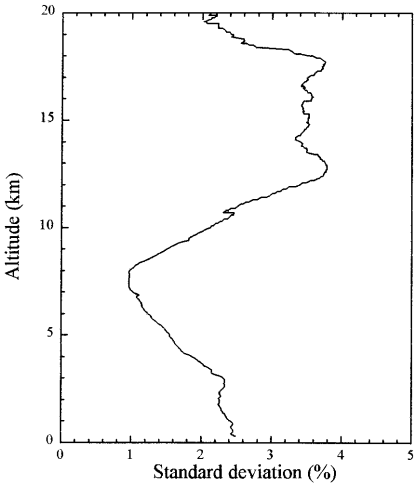

Fig. 2. Standard deviation of radiosonde molecular number densities with 66 radiosondes.

Then the number density profile is calculated downward and upward from the altitude of the reference number density. The number density at the isopycnic level varies ~2%.[32] The reference temperature comes from the USSA76 temperature profile data at 25 km. The sensitivities of the temperature derivations to these values are presented in Section 6.

The radiosonde temperatures were assumed to be the true atmospheric temperature. Nighttime radiosonde temperatures are accurate to within ±0.2 K at 100 mbars (~15 km) and to within ±0.6 K at 30 mbars (~24 km).[35] The rms differences were calculated over an altitude range of 5–10 km so that only upper tropospheric temperatures were used. Bias or systematic differences were also calculated.

B. Data Results

Figure 3 is a temperature profile that we derived from the Raman nitrogen signal using the molecular transmission term but with the aerosol transmission set to 1. Figure 3 also shows the radiosonde temperature profile for comparison purposes. This profile was chosen as an example of a temperature profile derivation because it was one of the few times that the radiosonde went as high as 25 km coincident with SRL measurements. The temperature difference between the lidar and the radiosonde profiles at 15 km is ~10 K. The rms difference between the lidar and the radiosonde temperatures in the altitude range of 5–10 km is 5.4 K, with a bias of −5.4 K. To reduce these temperature differences, we need to correct for extinction that is due to aerosols.

Using the USSA76 number density, we estimated an average lidar ratio for all 53 10-min profiles. For the calculations discussed here, the stratospheric aerosol layer for each profile began at an altitude where the scattering ratio was >1.1 (usually within the range of 13–16 km) and stopped at an altitude of 25 km. To reduce the error that was due to noise and variability in the aerosol content of the stratospheric aerosol layer, the average of all the calculated

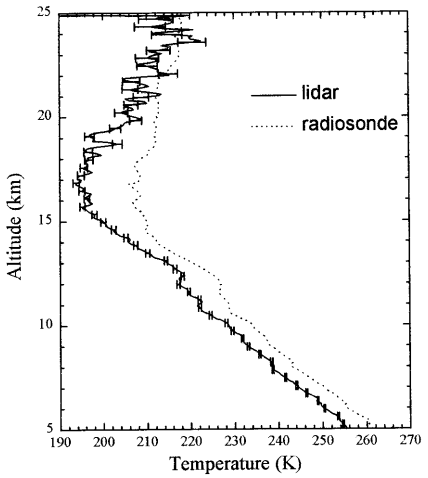

Fig. 3. Temperature profile that we derived from 19 November 1991, 0301–0310 UT data without using the aerosol transmission term. The rms difference between the two profiles was 5.4 K for an altitude range of 5–10 km. The corresponding bias was −5.4 K. The temperature data from a radiosonde launched at 0330 UT are also plotted for comparison.

lidar ratios was used for all subsequent temperature profile calculations.

The average value of the lidar ratio from the 53 profiles was 23.6 with a standard deviation of 8.0. This value can be compared to a range of 18–28 (Ref. 36) in Ferrare *et al.*[2] and a range of 15–60, with most of the ratios in the range of 20–30 in Ansmann *et al.*[31] The good agreement among these ratio values confirms the validity of our estimate.

By applying the aerosol transmission for the number density to the data in Fig. 3, we derived a new temperature profile in Fig. 4. (Compare Figs. 3 and 4 with Fig. 1, the aerosol backscattering ratio profile.) The temperature profile from the radiosonde that was launched at 0330 UT is also shown. The rms difference over a 5–10-km altitude range has been

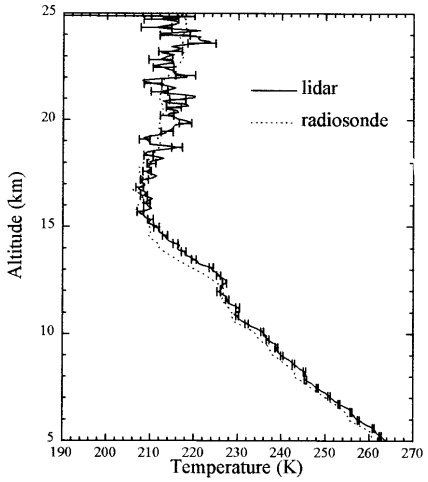

Fig. 4. Same as Fig. 3, except that the temperature profile used the aerosol transmission term with an aerosol extinction-to-backscatter ratio of 23.6. The rms error was 1.8 K with a bias error of 1.7 K.

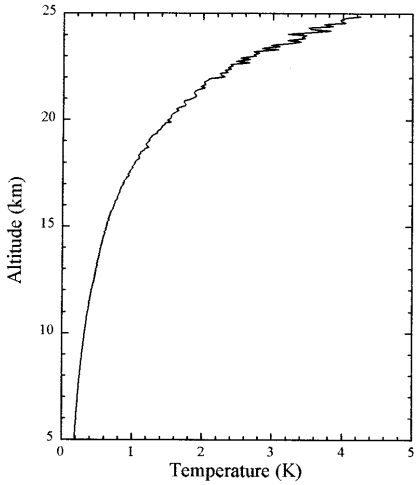

Fig. 5. Lidar random error profile as a function of altitude with Poisson statistics for data shown in Fig. 4.

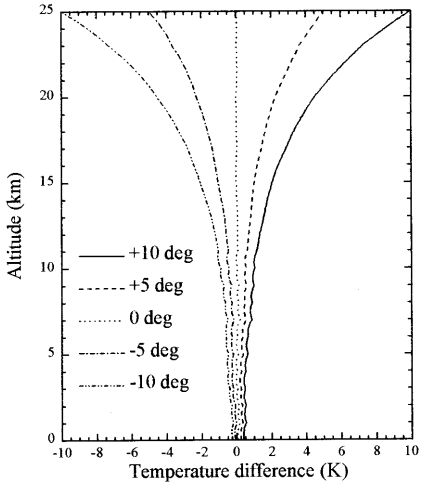

Fig. 6. Curves are the difference between the derived temperature profile and the USSA76 temperature profile. The temperature profiles were derived with the USSA76 number densities, starting with reference temperatures that differed from the 25-km U.S. Standard Atmosphere temperature by 0, ±5, and ±10 deg. Note that the profile derived from the 0-deg reference temperature difference has a 0 degree difference from the U.S. Standard Atmosphere temperature profile (the lines overlay each other). Note also that all of the temperature difference profiles converge to zero.

reduced to 1.8 K with a bias of 1.7 K. Above 15 km, the lidar temperature profile is noisy, but between 5 and 12 km, the structures of the lidar and radiosonde temperature profiles follow each other closely.

With 13 lidar profiles that were cloud free and had no upper tropospheric aerosols, and where a radiosonde was launched within 30 min of the lidar profile interval, the average rms difference was 1.8 ± 1.7 K, with an average bias of 0.4 ± 1.9 K. The first error number is the random error propagated through the equations, and the second error number is the standard deviation of the random errors in the altitude range of 5–10 km for the profiles used in the average. Because the radiosonde moves with the wind, it could be kilometers away from the lidar at higher altitudes and measuring the temperature of a different part of the atmosphere—not the atmosphere directly over the lidar. This could lead to differences in temperature between the lidar and the radiosonde profiles. In the altitude range of 5–10 km, maximum temperature changes to 3.5 K were noted between radiosondes that were launched every 2–4 h.

The errors bars shown in Figs. 3 and 4 were derived from the lidar signal with Poisson statistics as mentioned in Subsection 4.B. Figure 5 is a profile of the temperature errors resulting from random error in the lidar signal. The error is 1 K at 18 km and decreases with decreasing altitude. Because errors that are due to the reference temperature and the reference number density were not included, the error bars are due solely to lidar random errors.

6. Sensitivity Analysis

A. Reference Temperature

A sensitivity analysis of the reference temperature is presented in Fig. 6. Starting with different reference temperatures (211.55, 216.55, 221.55, 226.55, and 231.55 K) and using the USSA76 number density profile, we plotted the differences between the derived temperature profiles and the actual temperature profiles in Fig. 6, showing that for a reference temperature of ±5(10), there is less than a 1 K error in the temperature profile below an altitude of 15(10) km.

The reference number density at the isopycnic level varies by approximately 2%.[32] Our modifying the reference number density by ±2% does not affect the temperature errors but may change the slope of the number density ratio. On average, this modification to the number density actually causes a slight increase (~0.2 K) in the average rms temperature differences between the lidar data and the radiosonde data.

Of the 66 radiosondes that were launched during the experiment, 12 reached altitudes of 25 km or more. The average radiosonde temperature at 25 km was 216.8 K with a standard deviation of 2.3 K, which differs from the USSA76 temperature at 25 km by ~5 K. As can be seen in Fig. 6, a reference temperature that differs from the actual temperature by 5 K has less than a 1-deg error in the temperature profile below 15 km.

If the radiosonde temperature at 25 km was used for the reference temperature for the 19 November 1991 profile, the rms difference was 1.5 K with a bias of 1.4 K. If the number density derived from the radiosonde data at 7.95 km was used for the reference number density, the rms difference was 1.6 K with a bias of −1.5 K. If both radiosonde reference values were used, the rms difference was 1.9 K with a bias of −1.8 K. Even though the radiosonde was launched within 30 min of the lidar profile with the radiosonde data used for the reference, we still obtained approximately 2-deg rms difference in the 5–10-km altitude range.

B. Lidar Ratio

It was assumed throughout our research that the lidar ratio was constant with altitude. If the profile is split into three layers, two layers split the stratospheric aerosol layer in half (15–20 and 20–25 km) and one layer encompasses the entire troposphere and part of the lower stratosphere (0–15 km), and if we modify the lidar ratio of any single layer by ±5, the rms difference between the lidar and radiosonde temperatures in the 5–10-km regime will change by ±0.7 K. If we change the lidar ratio (±5) in any two layers by the same value, the rms difference changes by ±1.2 K. If we change the lidar ratio in any two layers by the same value but opposite in sign, the rms difference changes by ±0.3 K. If we set the lidar ratio in the troposphere to zero and modify the two stratospheric layers' lidar ratio by ±5, the rms difference changes by ±0.6 K. In summary, if one assumes a nonconstant lidar ratio, the derived temperature only changes by approximately a degree.

To determine the sensitivity of the lidar ratio, we first modified the lidar ratio by ±5 and then determined the average rms difference between the lidar and radiosonde temperatures. This variation of the lidar ratio increased the average rms difference by less than 1 deg, from 1.8 to 2.7 K. Then the lidar ratio was optimized by iteration to minimize the rms difference between the lidar and the radiosonde data between the altitudes of 5–10 km, if we assume that the radiosonde temperatures are the true temperatures. The average rms difference obtained from this optimization was 0.7 deg with a standard deviation of 0.2 K, 1 deg less than the nonoptimized profiles, with a bias of 0.05 deg and a standard deviation of 0.04 K. Next, when we averaged the optimized lidar ratios of the 13 upper-tropospheric aerosol-free profiles, we obtained an average of 22.6, which can be compared with our 53-profile-average of 23.6. This confirms that the technique we used to estimate the lidar ratio was a good approximation. The use of this new lidar ratio (22.6 instead of 23.6) would not change the average rms difference significantly. However, this demonstrates that a better estimate of the lidar ratio would reduce the temperature differences to less than 1 K.

Figure 7 shows the lidar-to-radiosonde number density ratio corresponding to Fig. 4. A straight line is also plotted for reference. The plotting of the number densities in this manner allows small deviations from the radiosonde number densities to become more apparent. A constant number density ratio means that the calculated number density is proportional to the radiosonde number density, implying that the calculated number density is an accurate representation of the atmospheric number density as measured by the radiosonde. Note how the deviations from a straight line in Fig. 7 correspond to the temperature variations in Fig. 4. This shows the importance of one obtaining a constant lidar-to-radiosonde number density ratio. Comparing Fig. 7 with Fig. 1, one can see a large variation

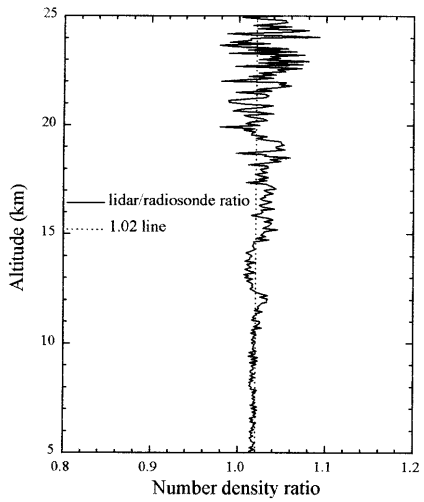

Fig. 7. Lidar-to-radiosonde number density ratio corresponding to Fig. 4. A straight line with a magnitude of 1.02 is plotted for reference. If the number density ratio is constant, then the lidar number density is proportional to the radiosonde measurements of number density. A decrease in the reference density by 2% shifts the entire profile to a line centered around 1.0.

in the aerosol backscattering ratio in the stratosphere. The variations at high altitudes could also be influenced by low S/N data.

C. Aerosol Backscattering Ratio

The aerosol backscattering ratio data were derived prior to the temperature calculations as mentioned above and need to be included when the errors are propagated through the equations. The error associated with the aerosol backscattering ratio is of the order of 1% at altitudes below 15 km, and the change in the temperature error was less than a tenth of a degree due to the inclusion of these errors.

The aerosol backscattering ratio was normalized with a minimum value that was estimated from data between the altitudes of 6 and 10 km. If this minimum value was not pure molecular scattering, then the lidar aerosol backscattering ratio will not be the true aerosol backscattering ratio of the atmosphere. This will increase the rms differences when the lidar aerosol backscattering ratio is used in the aerosol transmission term. If the aerosol backscattering were 10% of the Rayleigh backscattering (it was assumed to be zero), then the rms differences could increase by as much as 0.75 K. As mentioned above, the nearly constant aerosol backscattering ratio implies that backscattering at 351 nm is negligible and the errors in the aerosol backscattering ratio should be a few percent at most.[2]

Steinbrecht and Carswell[37] note that for 1991, γ, the wavelength dependence in Eqs. (9) and (12), should be approximately 2 and that this value should not be used for later years. If γ is allowed to range from 0–2, the average rms difference between the lidar and radiosonde temperature data changed by less than a tenth of a degree. The temperature al-

Table 1. Summary of Lidar Temperature Errors

Source of Error	Error (K)
Random signal error[a]	<1
Reference temperature[b]	<1
Average aerosol extinction-to-backscatter ratio ±5[c]	<1
Aerosol backscattering ratio	
Calibration constant[d]	~0.75
γ (wavelength ratio power)[c]	<0.1
Aerosol backscattering ratio error[c]	<0.1

[a]Below approximately 18 km.
[b]Below 15 km with a reference temperature within 5 deg of the real temperature at 25 km.
[c]Refers to the change in the average rms error.
[d]For a 10% error in the actual Rayleigh scattering.

gorithm is relatively insensitive to the value of γ, and γ = 1 was used.

D. Summary

Table 1 summarizes the errors associated with our derivation of a temperature profile in the upper troposphere. Not included in the table is the error induced by the wind-driven radiosonde measuring the temperature of a different part of the atmosphere than where the lidar is measuring. The largest errors are due to the reference temperature and the average aerosol extinction-to-backscatter ratio. If we integrate for longer time periods, the rms and bias differences decrease significantly because of the higher S/N ratio. A 20-min profile on 19 November 1991 resulted in a rms difference of 0.6 K with a bias of −0.2 K, more than a degree less than the 10-min profile rms difference and almost 2 deg less than the 10-min bias difference. We chose to use 10-min profiles here to show that temperatures can be derived in such a small time resolution.

The technique presented here is limited by the S/N ratio at the top of the profile, in this case 25 km. The data used in this study had S/N ratios that were greater than 20 at 25 km. S/N ratios of the order of 10 or less prevent a good estimation of the lidar ratio. Aerosol attenuation associated with aerosol backscattering ratios in the boundary layer greater than 1.5 or stratospheric aerosol backscattering ratios greater than 3.0 can cause low S/N ratios.

7. Conclusions

In the lower atmosphere after major volcanic eruptions, below 30 km, the molecular and aerosol transmissions must be applied to the number density calculation. To use the aerosol transmission, we calculated a lidar ratio by estimating the extinction of the lower stratospheric aerosol layer and dividing it by the integrated backscatter through the stratospheric aerosol layer. The reference number density and reference temperature came from the U.S. Standard Atmosphere 1976 model. After obtaining a number density profile, we calculated temperature profiles with a time resolution of 10 min and an altitude resolution of 300 m. The rms difference between lidar and radiosonde temperatures was <2 K over an altitude range of 5–10 km. This method can also be used to observe relative temperature changes over time.

The key to one obtaining temperature profiles with less than a degree error is in obtaining a number density profile that is proportional to the real atmospheric number density within 1%, as was shown by the sensitivity analysis. This could be done with data integrated for 20 min or with a more precise determination of the lidar ratio.

It was assumed throughout our research that the radiosonde temperatures were the true atmospheric temperatures. More than half of the radiosondes used in this analysis were Vaisala RS-80 radiosondes. In 1991, a small correction (0.2–0.4 deg) based on the vertical rise rate of the radiosonde was applied to the temperatures measured by the RS-80. In 1995, Schmidlin and Lee[35] determined that no correction was required for Vaisala radiosondes launched at night. This correction adds uncertainty as to what was the true atmospheric temperature profile. If rms differences were less than 1 K, then the SRL could have measured the true temperature profile and still have been different from the radiosonde temperature profile.

The authors extend their deepest appreciation to Frank Schmidlin, Prentice Moore, and Sam West of NASA/GSFC Wallops Flight Facility for radiosonde support and data, and to Glenn Staley, recently retired from NASA/GSFC's Experimental Instrumentation Branch, for his assistance during operations. The authors also thank the reviewers for their detailed comments. K. D. Evans and R. A. Ferrare are under contract to NASA/GSFC from Hughes STX Corp., Lanham, Maryland.

References and Note

1. S. H. Melfi, D. Whiteman, R. Ferrare, and K. Evans, "Raman lidar measurements of water vapor and aerosol/clouds during the FIRE/SPECTRE field campaign," in *16th International Laser Radar Conference*, NASA Conf. Publ. 3158, Part 2 (NASA, Hampton, Va., 1992), pp. 663–666.
2. R. A. Ferrare, S. H. Melfi, D. N. Whiteman, and K. D. Evans, "Raman lidar measurements of Pinatubo aerosols over southeastern Kansas during November-December 1991," Geophys. Res. Lett. **19,** 1599–1602 (1992).
3. A. Hauchecorne and M. L. Chanin, "Density and temperature profiles obtained by lidar between 35 and 70 km," Geophys. Res. Lett. **7,** 565–568 (1980).
4. M. L. Chanin and A. Hauchecorne, "Lidar observation of gravity and tidal waves in the middle atmosphere," J. Geophys. Res. **86,** 9715–9721 (1981).
5. C. R. Philbrick, F. J. Schmidlin, K. U. Grossman, G. Lange, D. Offermann, K. D. Baker, D. Krankowsky, and U. von Zahn, "Density and temperature structure over northern Europe," J. Atmos. Terr. Phys. **47,** 159–172 (1985).
6. T. Shibata, M. Kobuchi, and M. Maeda, "Measurements of density and temperature profiles in the middle atmosphere with a XeF lidar," Appl. Opt. **25,** 685–688 (1986).
7. G. Megie, "Lidar measurements of stratospheric temperature," in *Workshop on Early Detection of Changes in Stratospheric Structure* (NOAA, Boulder, Colo., March 1986), pp. 188–191.
8. D. B. Jenkins, D. P. Wareing, L. Thomas, and G. Vaughan, "Upper stratospheric and mesospheric temperatures derived

from lidar observations at Aberystwyth," J. Atmos. Terr. Phys. **49,** 287–298 (1987).
9. A. Hauchecorne, M. L. Chanin, and R. Wilson, "Mesospheric temperature inversion and gravity wave breaking," Geophys. Res. Lett. **14,** 933–936 (1987).
10. C. R. Philbrick, D. P. Sipler, G. Davidson, and W. P. Moskovitz, "Remote sensing of structure properties in the middle atmosphere using lidar," in *Laser and Optical Remote Sensing: Instrumentation and Techniques*, Vol. 18 of OSA 1987 Technical Digest Series (Optical Society of America, Washington, D.C., 1987), pp. 120–123.
11. C. R. Philbrick, "Lidar profiles of atmospheric structure properties," in *Earth and Atmospheric Remote Sensing*, R. J. Curran, J. A. Smith, and K. Watson, eds. Proc. SPIE **1492,** 76–84 (1991).
12. A. Adriani, G. P. Gobbi, F. Congeduti, and G. Di Donfrancesco, "Lidar observations of stratospheric and mesospheric temperature: November 1988-November 1989," Ann. Geophys. **9,** 252–258 (1991).
13. A. I. Carswell, S. R. Pal, W. Steinbrecht, J. A. Whiteway, A. Ulitsky, and T. Y. Wand, "Lidar measurements of the middle atmosphere," Can. J. Phys. **69,** 1076–1086 (1991).
14. R. A. Ferrare, T. J. McGee, D. Whiteman, J. Burris, M. Owens, J. Butler, R. A. Barnes, F. Schmidlin, W. Komhyr, P. H. Wang, M. P. McCormick, and A. J. Miller, "Lidar measurements of stratospheric temperature during STOIC," J. Geophys. Res. **100,** 9303–9312 (1995).
15. R. E. Bills and C. S. Gardner, "Lidar observations of the mesopause region temperature structure at Urbana," J. Geophys. Res. **98,** 1011–1021 (1993).
16. O. Uchino and I. Tabata, "Mobile lidar for simultaneous measurements of ozone, aerosols, and temperature in the stratosphere," Appl. Opt. **30,** 2005–2012 (1991).
17. J. W. Merriwether, P. D. Dao, R. T. McNutt, and W. Klemeti, "Rayleigh lidar observations of mesospheric temperature structure," J. Geophys. Res. **99,** 16,973–16,987 (1994).
18. J. Qian and C. S. Gardner, "Simultaneous lidar measurements of mesospheric Ca, Na, and temperature profiles at Urbana, Illinois," J. Geophys. Res. **100,** 7453–7461 (1995).
19. J. A. Whiteway and A. I. Carswell, "Lidar observations of gravity wave activity in the upper stratosphere over Toronto," J. Geophys. Res. **100,** 14,113–14,124 (1995).
20. G. Vaughan, D. P. Wareing, S. J. Pepler, L. Thomas, and V. Mitev, "Atmospheric temperature measurements made by rotational Raman scattering," Appl. Opt. **32,** 2758–2764 (1993).
21. D. Nedeljkovic, A. Hauchecorne, and M.-L. Chanin, "Rotational Raman lidar to measure the atmospheric temperature from the ground to 30 km," IEEE Trans. Geosci. Remote Sensing **31,** 90–101 (1993).
22. A. Hauchecorne, M. L. Chanin, P. Keckhut, and D. Nedeljkovic, "Lidar monitoring of the temperature in the middle and lower atmosphere," Appl. Phys. B **55,** 29–34 (1992).
23. S. H. Melfi and D. Whiteman, "Lower atmospheric temperature profile measurements using a raman lidar," in *13th International Laser Radar Conference*, NASA Conf. Publ. 2431 (NASA, Hampton Va., 1986), p. 188.
24. R. A. Ferrare, D. N. Whiteman, and S. H. Melfi, "Raman lidar measurements of temperature in the troposphere and lower stratosphere," in Optical Remote Sensing of the Atmosphere, Vol. 5 of 1990 OSA Technical Digest Series (Optical Society of America, Washington, D.C., 1990), pp. 508–511.
25. R. J. Alvarez II, L. M. Caldwell, P. G. Wolyn, D. A. Krueger, T. B. McKee, and C. Y. She, "Profiling temperature, pressure, and aerosol properties using a high spectral resolution lidar employing atomic blocking filters," J. Atmos. Oceanic Technol. **10,** 546–556 (1993).
26. T. Kobayashi and T. Yamada, "Tropospheric temperature sensing by the Raman and Rayleigh-Mie lidar using UV excimer lasers," in *14th International Laser Radar Conference* (Istituto di Ricerca Sulle Onde Elettromagnetiche, CNR, Firenze, Italy, 1988), pp. 67–69.
27. J. D. Klett, "Stable analytic inversion solution for processing lidar returns," Appl. Opt. **20,** 211–220 (1981).
28. P. Keckhut, M. L. Chanin, and A. Hauchecorne, "Stratospheric temperature measurement using Raman lidar," Appl. Opt. **29,** 5182–5186 (1990).
29. D. N. Whiteman, S. H. Melfi, and R. A. Ferrare, "Raman lidar system for the measurement of water vapor and aerosols in the Earth's atmosphere," Appl. Opt. **31,** 3068–3082 (1992).
30. D. N. Whiteman, R. A. Ferrare, S. H. Melfi, and K. D. Evans, "Solar blind scattering measurements of water vapor using a KrF Excimer," in *Optical Remote Sensing of the Atmosphere*, Vol. 5 of 1993 OSA Technical Digest Series (Optical Society of America, Washington, D.C., 1993), pp. 165–168.
31. A. Ansmann, M. Riebesell, U. Wandinger, C. Weitkamp, W. Lahmann, and W. Michaelis, "Combined Raman elastic-backscatter LIDAR for vertical profiling of moisture, aerosol extinction, backscatter, and LIDAR ratio," Appl. Phys. B **55,** 18–28 (1992).
32. National Oceanic and Atmospheric Administration, *U.S. Standard Atmosphere* (U.S. Government Printing Office, Washington, D.C., 1976), p. 26.
33. J. F. Kaiser and W. A. Reed, "Data smoothing using low pass filters," Rev. Sci. Instrum. **48,** 1447–1457 (1977).
34. P. R. Bevington, *Data Reduction and Error Analysis for the Physical Sciences* (McGraw-Hill, New York, 1969), p. 64.
35. F. J. Schmidlin, H. S. Lee, and B. Runganayakamma, "Deriving the accuracy of different radiosonde types using the three-thermistor radiosonde technique," in *Proceedings of Ninth Symposium on Meteorological Observations and Instrumentation* (American Meteorological Society, Boston, Mass., 1995), pp. 27–31.
36. Ferrare *et al.*[2] calculated the aerosol extinction-to-backscatter ratio from the derived aerosol extinction and scattering ratio profiles using density profiles derived from radiosondes and then performed an average through the stratospheric aerosol layer. This method was completely different from the estimation presented here with the same data set.
37. W. Steinbrecht and A. I. Carswell, "Evaluation of the effects of Mount Pinatubo aerosol on differential absorption lidar measurements of stratospheric ozone," J. Geophys. Res. **100,** 1215–1234 (1995).